LETTER

https://doi.org/10.1038/s41586-018-0661-6

Emergence of multi-body interactions in a fermionic lattice clock

A. Goban[1,2,7]*, R. B. Hutson[1,2,7], G. E. Marti[1,2,6], S. L. Campbell[1,2,4,5], M. A. Perlin[1,2], P. S. Julienne[3], J. P. D'Incao[1,2], A. M. Rey[1,2] & J. Ye[1,2]*

Alkaline-earth atoms have metastable 'clock' states with minute-long optical lifetimes, high-spin nuclei and SU(N)-symmetric interactions, making them powerful platforms for atomic clocks[1], quantum information processing[2] and quantum simulation[3]. Few-particle systems of such atoms provide opportunities to observe the emergence of complex many-body phenomena with increasing system size[4]. Multi-body interactions among particles are emergent phenomena, which cannot be broken down into sums over underlying pairwise interactions. They could potentially be used to create exotic states of quantum matter[5,6], but have yet to be explored in ultracold fermions. Here we create arrays of isolated few-body systems in an optical clock based on a three-dimensional lattice of fermionic ^{87}Sr atoms. We use high-resolution clock spectroscopy to directly observe the onset of elastic and inelastic multi-body interactions among atoms. We measure the frequency shifts of the clock transition for varying numbers of atoms per lattice site, from $n=1$ to $n=5$, and observe nonlinear interaction shifts characteristic of elastic multi-body effects. These measurements, combined with theory, elucidate an emergence of SU(N)-symmetric multi-body interactions, which are unique to fermionic alkaline-earth atoms. To study inelastic multi-body effects, we use these frequency shifts to isolate n-occupied sites in the lattice and measure the corresponding lifetimes of the clock states. This allows us to access the short-range few-body physics without experiencing the systematic effects that are encountered in a bulk gas. The lifetimes that we measure in the isolated few-body systems agree very well with numerical predictions based on a simple model for the interatomic potential, suggesting a universality in ultracold collisions. By connecting these few-body systems through tunnelling, the favourable energy and timescales of the interactions will allow our system to be used for studies of high-spin quantum magnetism[7,8] and the Kondo effect[3,9].

Fermionic alkaline-earth and alkaline-earth-like atoms have $^1S_0$ ground clock states and metastable $^3P_0$ excited clock states ($^3P_0$ has a lifetime of roughly 160 s in ^{87}Sr), which provide two (electronic) orbital degrees of freedom that are largely decoupled from the nuclear spin I. This decoupling gives rise to orbital, SU($N=2I+1$)-symmetric, two-body interactions in which the s-wave and p-wave scattering parameters are independent of the nuclear spin state[3,8]. This degeneracy can be quite large ($I=9/2$ for ^{87}Sr), enabling studies of quantum states of matter with no direct analogues in nature, such as the SU(N) Mott insulator[3,10,11]. Two-orbital, SU(N)-symmetric interactions were first observed directly using clock spectroscopy[7,12,13] and have since provided new opportunities for studying strongly interacting Fermi gases[14,15] and the Kondo lattice model[9].

Whereas particles microscopically interact in a pairwise manner, multi-body interactions can emerge in a low-energy effective field theory in which fluctuations beyond some length or momentum scale are integrated out. Examples of such multi-body interactions include three-nucleon forces[16] and some fractional quantum Hall states[5]. Multi-body interactions have been predicted to arise in various optical lattice experiments[6,17] and have been observed in bosonic systems[18,19]. Although a single impurity interacting with a few identical fermions has been studied[4], multi-body interactions in high-spin fermions have yet to be explored.

In ultracold gases, the effects of multi-body interactions have been explored extensively in the context of three-body recombination processes[20], including in studies of exotic Efimov states and of other forms of universality associated with long-range interactions[21,22]. However, comparison to theory is often difficult owing to the bulk-gas nature of these experiments. Improved control and understanding of the external degrees of freedom of atoms is crucial for testing theoretical models of ultracold collisions[23,24].

Here we study the emergence of multi-body interactions by combining isolated few-body systems in an optical lattice with high-resolution clock spectroscopy. In our experiment, the ultracold gas is prepared similarly to previous work[25,26]. In summary, we prepare a ten-spin-component Fermi degenerate gas, with atoms distributed equally among all nuclear spin states. We typically produce 10^3–10^4 atoms per nuclear spin state at a temperature $T=10$–20 nK $=0.1T_F$, where T_F is the Fermi temperature. The gas is loaded into a nearly isotropic, three-dimensional optical lattice, in which the geometric mean of the trap depths for the three lattice beams $\mathcal{U}$ varies from $30E_{rec}$ to $80E_{rec}$, where $E_{rec}=h\times 3.5$ kHz is the recoil energy of a lattice photon and h is the Planck constant. At these trap depths, there is negligible tunnelling between neighbouring sites over the timescale of the experiment.

As depicted in Fig. 1a, for atoms in doubly occupied sites, a π-polarized clock photon resonantly couples the ground state $|gg\rangle$ to the orbitally symmetric (or orbitally antisymmetric) excited state $|eg^+\rangle$ (or $|eg^-\rangle$) upon matching the detuning $(E_{eg^+}-E_{gg})/h$ (or $(E_{eg^-}-E_{gg})/h$) at zero magnetic field. Here, 'g' and 'e' represent the ground clock state $^1S_0$ and the excited clock state $^3P_0$, respectively, and E_X is the on-site interaction energy for $X\in\{gg, eg^\pm\}$. Similarly, for sites with $n\geq 3$, the ground state $|g\cdots\rangle$ can be driven to the orbitally symmetric state $|eg\cdots^+\rangle$ or to the state $|eg\cdots^-\rangle$, for which the orbital and nuclear spin degrees of freedom are not separable. The π-polarized clock light preserves the initial distribution of the nuclear spin states.

We spatially resolve the spectroscopic signal using absorption imaging[26] and the readout scheme presented in Fig. 1b. We measure the differential interaction energies and the spatial distributions of each occupation number[27,28]. In Fig. 2a we show sample spectra of a ten-spin-component Fermi gas using 20-ms clock pulses from a 26-mHz-line width ultrastable laser. For each occupation number n, there is a pair of single-excitation resonances, labelled $n^\pm$, which correspond to the two sets of final states $|eg\cdots^\pm\rangle$. SU(N) symmetry and fermionic antisymmetrization dictate that only two eigenenergies appear for each n-atom sample (see Supplementary Information).

In Fig. 2b we show the column density of different occupation numbers for a sample of 2×10^5 atoms. The shells of decreasing size with

[1]JILA, National Institute of Standards and Technology, University of Colorado, Boulder, CO, USA. [2]Department of Physics, University of Colorado, Boulder, CO, USA. [3]Joint Quantum Institute, NIST, University of Maryland, Gaithersburg, MD, USA. [4]Present address: Molecular Biophysics and Integrated Bioimaging, Lawrence Berkeley National Laboratory, Berkeley, CA, USA. [5]Present address: Department of Physics, University of California, Berkeley, CA, USA. [6]Present address: Department of Molecular and Cellular Physiology, Stanford University, Stanford, CA, USA. [7]These authors contributed equally: A. Goban, R. B. Hutson. *e-mail: Akihisa.Goban@jila.colorado.edu; Ye@jila.colorado.edu

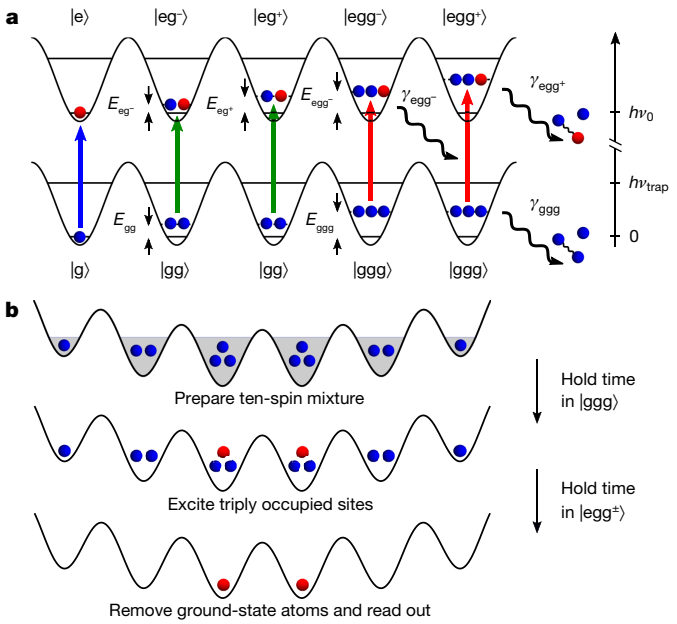

Fig. 1 | Two-orbital interactions in a three-dimensional lattice and experimental sequence. a, One to three ^{87}Sr atoms (blue and red circles for electronic ground- and excited-state atoms, respectively) occupy the lowest motional state of a lattice site, with corresponding on-site energies E_X. We use a state-independent lattice that operates at the 'magic' wavelength, at which the polarizabilities of the ground and excited states are identical. In a deep three-dimensional lattice, each site can be regarded as an isolated few-body system with a trap frequency ν_{trap}. A clock photon resonantly couples the ground state $|g\cdots\rangle$ to the single-excitation manifold $|eg\cdots^{\pm}\rangle$, leading to a spectroscopic shift from the bare resonance frequency $\nu_0 \approx 429$ THz. Multi-body interactions manifest in sites with three or more atoms, both in the observed clock shifts and in their decay (black squiggly arrows) into a diatomic molecule plus a free atom at a rate γ_X. **b**, Experimental sequence for imaging triply occupied sites. A ten-nuclear-spin mixture is loaded into a three-dimensional optical lattice. A clock pulse resonantly drives triply occupied sites $|ggg\rangle$ to an excited state $|egg^{\pm}\rangle$. After all atoms in the ground state are removed, the remaining atoms, in the excited state, are read out using absorption imaging. Three-body decay rates are measured by adding a hold time before (for γ_{ggg}) or after (for $\gamma_{egg^{\pm}}$) applying the clock pulse.

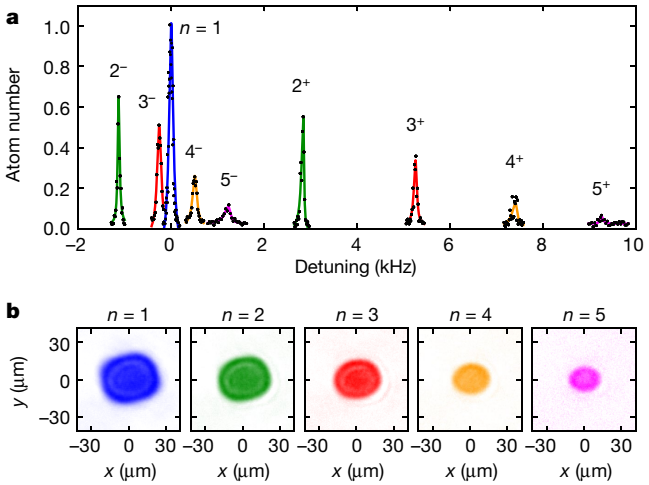

Fig. 2 | Clock spectroscopy of a ten-component Fermi gas in a three-dimensional lattice. a, Overlayed clock spectra for occupation numbers $n = 1, \ldots, 5$ at a mean trap depth of $\mathcal{U} = 54E_{rec}$ ($\nu_{trap} = 51$ kHz). The labels $n^{\pm}$ denote the excitation $|eg\cdots^{\pm}\rangle$ for n-occupied sites. For large occupations, the line shapes become asymmetric owing to the inhomogeneity of the trap depth. The solid lines are fits used to determine the resonance frequencies (see Methods). The detunings are given relative to the resonance of the clock transition for singly occupied sites (blue) and the atom number is normalized such that the peak height for singly occupied sites is unity. Each data point is the result of a single experimental cycle. **b**, Column densities of different occupation numbers for a sample of 2×10^5 atoms. The absorption images for different occupation numbers were obtained according to the procedure in Fig. 1b, by first exciting the symmetric resonances. Each image is averaged over 20 experimental cycles.

increasing occupation number are a result of balancing the external confinement generated by Gaussian lattice beams with the on-site interaction energies. As observed for small n, larger clouds of atoms extend over areas where the trapping frequencies are relatively lower, resulting in smaller on-site interaction energies. To eliminate a possible systematic shift from the changing cloud size, we adjust the final evaporation point to maximize the central density of the desired occupation number and measure the spectroscopic response in only the central $4\,\mu m \times 4\,\mu m \times 2\,\mu m$ region of the trap. The vertical plane is selected by loading the lattice from a trap that is tightly confining against gravity, loading only a 2-μm-thick vertical region. Spatial selection in the horizontal plane is performed by spatially filtering the images, measuring the response from only the central region of the lattice. The trap depth in the central region of the lattice is calibrated via motional sideband spectroscopy of an $n = 1$ sample with the same spatial selection.

To investigate multi-body interactions in multiply occupied sites, we consider the case of two interacting fermionic atoms, each with two internal degrees of freedom: an electronic orbital, $x \in \{g, e\}$, and a nuclear spin sublevel, $m \in \{-I, -I+1, \ldots, I\}$. The interactions depend on only the electronic degree of freedom, so all s-wave scattering processes are parameterized by four scattering lengths a_X, with $X \in \{gg, eg^+, eg^-, ee\}$, resulting in SU($N$)-symmetric properties of the system. Here, '+' ('−') denotes a symmetric (antisymmetric) superposition of the electronic orbitals. In our experiments, atoms are trapped in the motional ground states of deep lattice sites with a single-particle Wannier function $\phi_0(\boldsymbol{r})$, localized to a characteristic length scale l_0. Because all atoms are in the motional ground states, the Pauli exclusion principle requires that atoms with the same orbital state x have different nuclear spins m. Here, we consider the case in which each atom is in a different spin state.

In the limit of weak interactions ($l_0 \gg |a_X|$), the pairwise interaction energy can be expressed as

$$U_X^{(2)} = \frac{4\pi\hbar^2}{m_a} a_X \int |\phi_0(\boldsymbol{r})|^4 \, \mathrm{d}^3\boldsymbol{r}$$

where m_a is the atomic mass and $\hbar = h/(2\pi)$. In this regime, the on-site many-body Hamiltonian is

$$H = \sum_{m \neq m'} \left[\frac{U_{gg}^{(2)}}{2} n_{g,m} n_{g,m'} + \frac{U_{ee}^{(2)}}{2} n_{e,m} n_{e,m'} + V_{ex}^{(2)} c_{e,m}^{\dagger} c_{g,m}^{\dagger} c_{e,m'} c_{g,m} \right] \quad (1)$$

where $c_{x,m}^{\dagger}$ ($c_{x,m}$) creates (destroys) an atom in orbital $x \in \{e, g\}$ with spin m, and $n_{x,m} = c_{x,m}^{\dagger} c_{x,m}$. The direct and exchange interaction energies are $V^{(2)} = (U_{eg^+}^{(2)} + U_{eg^-}^{(2)})/2$ and $V_{ex}^{(2)} = (U_{eg^+}^{(2)} - U_{eg^-}^{(2)})/2$, respectively. For a lattice site occupied by n atoms, the Hamiltonian in equation (1) has a ground state $|g\cdots\rangle$ with a corresponding eigenenergy $E_{g\cdots}^{(2)}$ and a manifold of singly excited states with two distinct eigenenergies $E_{eg\cdots,\pm}^{(2)}$, one for the orbitally symmetric states $|eg\cdots^{+}\rangle$ and the other for the $(n-1)$-fold-degenerate states $|eg\cdots^{-}\rangle$. The states $|g\cdots\rangle$ and $|eg\cdots^{+}\rangle$ are each symmetric in their orbital degree of freedom and, as such, fermionic statistics requires their nuclear spin degree of freedom to form an SU(N) singlet. The orbital degree of freedom of $|eg\cdots^{+}\rangle$ is an n-body W state, which constitutes an important resource for quantum information processing and quantum communications protocols[29]. For $n \geq 3$, the $|eg\cdots^{-}\rangle$ states are highly entangled between their orbital and nuclear spin degrees of freedom such that each degree of freedom is of mixed symmetry (see Supplementary Information).

Table 1 | s-Wave scattering lengths and three-body loss coefficients

Channel, X	s-Wave scattering lengths, a_X (a_0)	Two-body loss coefficients, β_X (10^{-16} cm^3 s^{-1})
gg	96.2(0.1)	
eg$^-$	69.1(0.2)$_{stat}$(0.9)$_{sys}$	≤2.1(0.2)
eg$^+$	161.3(0.5)$_{stat}$(2.5)$_{sys}$	≤2.5(0.3)
Channel, X	**Three-body loss coefficients, β_X (10^{-30} cm^3 s^{-1})**	
	Measured	**Calculated**
ggg	2.0(0.2)	1.7
egg$^-$	25(1)	26
egg$^+$	15(1)	8.0

The scattering length of ground states $a_{gg} = 96.2(0.1)a_0$ is determined from photoassociation spectroscopy[30]; all the other values are from this work. The measured elastic s-wave scattering lengths a_X are consistent with previously reported values[7], with an improvement by a factor of ten in the uncertainty for $X = eg^-$. The subscripts 'stat' and 'sys' denote the statistical and systematic uncertainty, respectively (see Supplementary Information). The two-body loss coefficients β_X are upper bounds, limited by the excited-state lifetime. The measured three-body loss coefficients are in good agreement with the ones calculated using a universal van der Waals model.

For tighter confinement and stronger on-site interactions—that is, if a_X/l_0 is not negligible—corrections to equation (1) become increasingly important. The increased interaction energy facilitates off-resonant transitions to higher motional states. Equivalently, the spatial wavefunction $\phi_0(\boldsymbol{r})$ becomes dependent on the number of atoms per site and their configuration. This effect can be captured by a lowest-band effective Hamiltonian where the higher motional states are integrated out, with two consequences: (i) the two-body interaction energies are characterized by an in-trap scattering length, rescaled from the free-space one; and (ii) the total interaction energy for $n \geq 3$ atoms cannot be broken down into a sum over pairs of atoms[17], leading to effective multi-body interactions. Considering at most one atom in the excited state, equation (1) must be modified to include multi-body corrections:

$$H' = \sum_{m \neq m' \neq m''} [\frac{U^{(3)}_{ggg}}{6} n_{g,m} n_{g,m'} n_{g,m''} + \frac{V^{(3)}}{2} n_{e,m} n_{g,m'} n_{g,m''} + \frac{V^{(3)}_{ex}}{2} c^{\dagger}_{e,m} c^{\dagger}_{g,m} c_{e,m} c_{g,m'} n_{g,m''}] + \mathcal{O}(n^4) \quad (2)$$

where $U^{(3)}_{ggg}$, $V^{(3)}$ and $V^{(3)}_{ex}$ are the effective three-body ground-state, direct and exchange interaction energies. Owing to the SU(N) symmetry, H' has the same eigenstates as H, but with modified n-body eigenenergies (see Supplementary Information). These multi-body interactions can be probed by spectroscopically addressing lattice sites with different occupation numbers.

To extract the multi-body effects from equation (2), we measure the frequency shifts $(E_{eg^{\pm}} - E_{gg})/h$ for various mean trap depths. By incorporating the corrections due to lattice confinement with a previous measurement of the ground-state scattering length $a_{gg} = 96.2(0.1)a_0$, where a_0 is the Bohr radius[30], we extract the free-space scattering lengths $a_{eg^{\pm}}$, shown in Table 1 (see Supplementary Information).

Multi-body interactions occur only at sites with three or more atoms and cause frequency shifts that are nonlinear in the occupation number n. The measured clock shifts of the $|eg\cdots^{\pm}\rangle$ branches are shown as red points in Fig. 3a, b. These clock shifts deviate from the values expected from equation (1) (blue triangles), which are proportional to the occupation number n, and are consistent with the three-body corrections in equation (2) (black squares). These higher-order contributions (Fig. 3c, d) can be intuitively interpreted as broadening of the wavefunction, lowering the magnitude of the overall interaction energy. From a variational calculation, we find that the wavefunction for $n = 5$ atoms is broadened by about 8% relative to a non-interacting wavefunction.

Multi-body effects also appear in these few-body systems as three-body recombination loss. These losses occur when three atoms recombine to form a deeply bound diatomic molecule and a free atom, each carrying enough energy to eject it from the trap[24]. We selectively determine the lifetime of a given n-atom $|g\cdots\rangle$ state by holding atoms in a deep lattice for a variable time, then resonantly driving the transition $|g\cdots\rangle \rightarrow |eg\cdots^{\pm}\rangle$ to spectroscopically address only the n-atom sites, and finally measuring the excited-state atom population after removing the ground-state atoms, as illustrated in Fig. 1. Similarly, the loss rate of the $|eg\cdots^{\pm}\rangle$ state is determined by first driving the transition $|g\cdots\rangle \rightarrow |eg\cdots^{\pm}\rangle$, and then holding for a variable time before removing the ground-state atoms. Because this procedure measures the probability for the n-atom system to remain in its initial state, the spectroscopic signal decays in a simple and robust form as a single exponential, which we fit to extract a 1/e lifetime. This analysis is much simpler than that for bulk-gas experiments, for which decay curves must be fitted with multiple rate constants corresponding to one-, two- and three-body losses[31,32].

To disentangle these multi-body effects from inelastic two-body collisions, we measure the ground- and excited-state lifetimes of the one- and two-atom sites. Whereas we observe a vacuum-limited 1/e lifetime of around 100 s for the $|g\rangle$ and $|gg\rangle$ states, off-resonant Raman scattering from the optical lattice light causes a decay of the single-atom excited state, $|e\rangle \rightarrow |g\rangle$, with a time constant of 9.6(0.4) s at a mean trap depth of $\mathcal{U} = 73E_{rec}$ (R.B.H. et al., manuscript in preparation). Note that all errors for the lifetimes are 1 s.e. from exponential fits. At this same trap depth, we find the lifetimes $\tau_{eg^{\pm}}$ of the $|eg^+\rangle$ and $|eg^-\rangle$ states to be 5.1(0.7) s and 6.1(0.7) s, respectively. Such two-body lifetimes can be related to a two-body loss coefficient $\beta_{eg^{\pm}}$ via the expression

$$\tau^{-1}_{eg^{\pm}} = \beta_{eg^{\pm}} \int |\phi_0(\boldsymbol{r})|^4 \, d^3\boldsymbol{r}$$

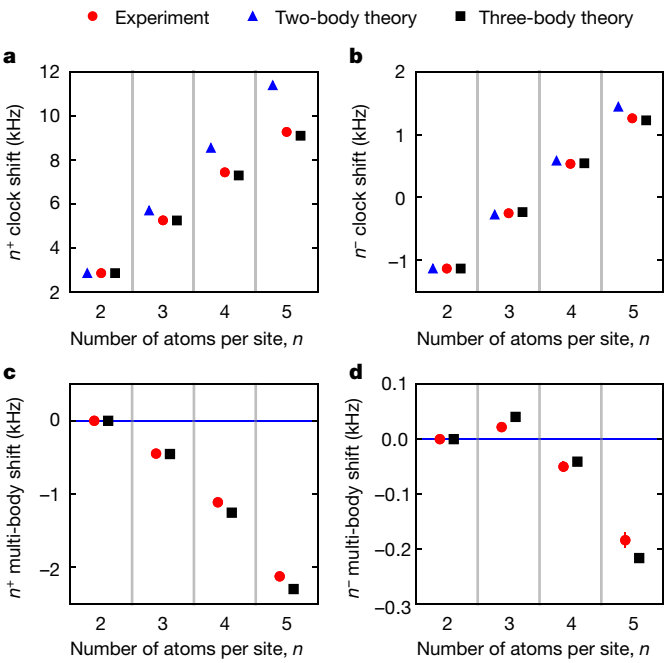

Fig. 3 | Effective multi-body clock shifts. a, Clock shifts of $|eg\cdots^{+}\rangle$ from $n = 2, \ldots, 5$ at a mean trap depth of $\mathcal{U} = 54E_{rec}$ ($\nu_{trap} = 51$ kHz). Effective multi-body interactions are observed in the experimental data (red circles) as a deviation from the two-body prediction (blue triangles). The calculated shifts from an effective Hamiltonian including three-body interactions (see text and Supplementary Information) are shown as black squares. The points at each occupation number n are offset horizontally for clarity. The uncertainties of the experimental data are smaller than the size of the symbols. **b**, Clock shifts of $|eg\cdots^{-}\rangle$ under the same conditions as in **a**. The two-body theory shows smaller deviations from the measured shifts at $n = 3$ and $n = 4$, owing to a near cancellation of the three-body shifts between $|g\cdots\rangle$ and $|eg\cdots^{-}\rangle$. **c**, **d**, Multi-body interaction shifts, which correspond to the data from **a** and **b** with two-body contributions subtracted. All error bars are 1 s.e., determined from fits of the resonance position.

However, because the two-body lifetimes are only slightly shorter than that of a single excited atom, we can determine only upper limits: $\beta_{\mathrm{eg}^+} \leq 2.5(0.3) \times 10^{-16}\,\mathrm{cm}^3\,\mathrm{s}^{-1}$ and $\beta_{\mathrm{eg}^-} \leq 2.1(0.2) \times 10^{-16}\,\mathrm{cm}^3\,\mathrm{s}^{-1}$. The measured lifetimes of the three-atom states, τ_X for $X \in \{\mathrm{ggg}, \mathrm{egg}^+, \mathrm{egg}^-\}$, at various mean trap depths are shown in Fig. 4a. These multi-body decays all occur on timescales much shorter than those of one- and two-body losses. Furthermore, the excited states are observed to decay faster than the ground state by approximately an order of magnitude. We attribute this to the increased number of molecular decay channels after replacing a ground-state atom with a distinguishable excited-state atom. Table 1 shows the density-independent three-body loss coefficient β_X extracted from these measurements via the expression

$$\tau_X^{-1} = \beta_X \int |\phi_0(\boldsymbol{r})|^6 \, \mathrm{d}^3\boldsymbol{r}$$

Next, we compare the measured three-body lifetimes to a model in which atoms interact by pairwise, additive, long-range van der Waals potentials joined at shorter range to a pseudopotential that is adjusted to yield, in each case, the measured two-body scattering lengths given in Table 1[7,24,33]. Numerically solving the three-body Schrödinger equation yields the frequency shifts and decay lifetimes for three atoms confined in a harmonic trap (see Supplementary Information). We increase the number of bound states in each pairwise potential until all results converge to less than 10%. As shown in Fig. 4a, the calculated lifetimes (open circles) are remarkably close to the measured lifetimes (filled circles) given the simplicity of our universal van der Waals model, which has no fit parameters. Whereas our results for $|\mathrm{ggg}\rangle$ and $|\mathrm{egg}^-\rangle$ agree with the observed lifetimes to within 15% or less, the results for $|\mathrm{egg}^+\rangle$ overestimate the lifetimes by about 50%, most probably owing to the fact that for this state our model does not allow for decay into all possible diatomic molecular states (see Supplementary Information). As a sanity check, the frequency shifts produced by this model agree with the measurements shown in Fig. 3a, b to within 10%, despite assuming a harmonic trap potential.

We extract three-body loss coefficients β_X from the calculated lifetimes using the same procedure as for the experimental results shown in Table 1. The good agreement between the universal van der Waals model and our ^{87}Sr lattice experiment is in sharp contrast to the disagreement, by a factor of 2–4, for bulk-gas ^{87}Rb experiments. The universal van der Waals model of ^{87}Rb gives a three-body loss rate coefficient of[24] $1.0 \times 10^{-29}\,\mathrm{cm}^6\,\mathrm{s}^{-1}$, in contrast to the measured value of[31] $4.3(1.8) \times 10^{-29}\,\mathrm{cm}^6\,\mathrm{s}^{-1}$. This scenario suggests that a lattice experiment with ^{87}Rb could greatly decrease the uncertainty in the ^{87}Rb three-body recombination loss coefficient and provide a better test of the theory for that system.

Finally, we study the dependence of the lifetimes on the occupation number. In Fig. 4b we show a

$$\tau_{g\cdots}^{-1} = \tau_{\mathrm{ggg}}^{-1} \binom{n}{3}$$

scaling of the lifetime of the n-body ground state for $n \geq 3$, which suggests that three-body loss remains the dominant mechanism. The lifetimes of the n-atom excited states, along with their expected scalings from counting the number of three-body loss channels, are shown in Fig. 4c (see Supplementary Information). These relatively long lifetimes are promising for future experiments involving coupled wells with large occupation numbers.

In conclusion, we have demonstrated two manifestations of multi-body interactions arising from pairwise interactions in few-body systems of fermions. Our spectroscopic technique, along with spatially resolved readout, enables efficient isolation of few-body systems, which prove to be ideal for observing multi-body effects. It also provides a simple way to create the highly entangled and long-lived states $|\mathrm{eg}\cdots^{\pm}\rangle$, a useful resource for quantum information processing[29]. The few-body systems enable precise measurements of the $a_{\mathrm{eg}^\pm}$ scattering lengths and the three-body loss rates which agree with the universal van der Waals model. The collisional parameters, in the case of ^{87}Sr, are found to be particularly suitable for studies of two-orbital SU(N) magnetism, which should arise in the presence of weak tunnelling. These interactions have been predicted to create long-sought states of matter, including valence-bond solids and chiral spin liquids[3].

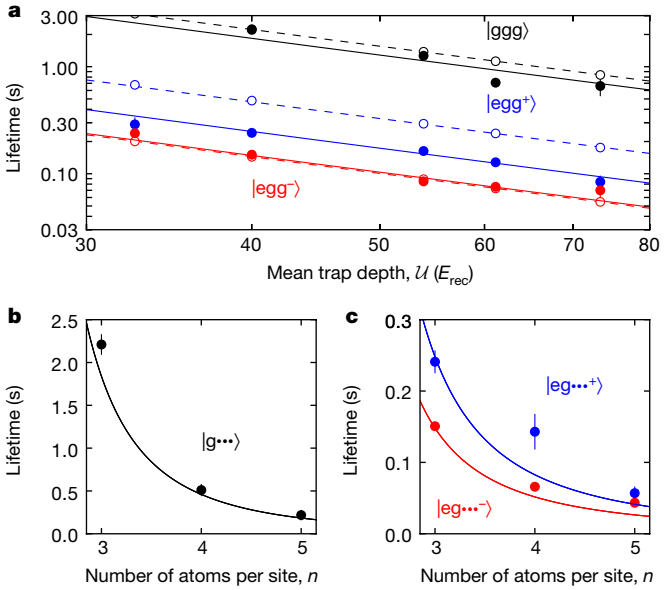

Fig. 4 | Three-body loss rate and occupation-number-dependent lifetime. a, Dependence of the $n = 3$ lifetimes on the mean trap depth for the $|\mathrm{ggg}\rangle$ (black), $|\mathrm{egg}^+\rangle$ (blue) and $|\mathrm{egg}^-\rangle$ (red) states. The measured lifetimes (filled circles) are close to the ones calculated from a universal van der Waals model (open circles; see text and Supplementary Information). From the fits shown as solid (dashed) lines, we extract the three-body loss coefficients β_X for the measured (calculated) lifetimes, which are summarized in Table 1. The lifetime of $|\mathrm{ggg}\rangle$ is ten times that of $|\mathrm{egg}^\pm\rangle$, because the number of molecular states increases owing to one distinguishable particle in the excited state. **b**, **c**, Dependence of the lifetimes of the $|\mathrm{g}\cdots\rangle$ and $|\mathrm{eg}\cdots^\pm\rangle$ states on the occupation number n at $\mathcal{U} = 40E_{\mathrm{rec}}$. The solid lines are the lifetimes calculated assuming pure three-body losses, with the measured β_{ggg} and $\beta_{\mathrm{egg}^\pm}$ values as input parameters (see text and Supplementary Information). All error bars are 1 s.e., determined from exponential fits.

Online content

Any methods, additional references, Nature Research reporting summaries, source data, statements of data availability and associated accession codes are available at https://doi.org/10.1038/s41586-018-0661-6.

Received: 15 March 2018; Accepted: 20 August 2018;
Published online 31 October 2018.

1. Ludlow, A. D., Boyd, M. M., Ye, J., Peik, E. & Schmidt, P. O. Optical atomic clocks. *Rev. Mod. Phys.* **87**, 637–701 (2015).
2. Daley, A. J. Quantum computing and quantum simulation with group-II atoms. *Quantum Inform. Process.* **10**, 865–884 (2011).
3. Cazalilla, M. A. & Rey, A. M. Ultracold Fermi gases with emergent SU(*N*) symmetry. *Rep. Prog. Phys.* **77**, 124401 (2014).
4. Wenz, A. N. *et al*. From few to many: observing the formation of a Fermi sea one atom at a time. *Science* **342**, 457–460 (2013).
5. Fradkin, E. H., Nayak, C., Tsvelik, A. & Wilczek, F. A Chern-Simons effective field theory for the Pfaffian quantum Hall state. *Nucl. Phys. B* **516**, 704–718 (1998).
6. Büchler, H. P., Micheli, A. & Zoller, P. Three-body interactions with cold polar molecules. *Nat. Phys.* **3**, 726–731 (2007).
7. Zhang, X. *et al*. Spectroscopic observation of SU(*N*)-symmetric interactions in Sr orbital magnetism. *Science* **345**, 1467–1473 (2014).
8. Gorshkov, A. V. *et al*. Two-orbital SU(*N*) magnetism with ultracold alkaline-earth atoms. *Nat. Phys.* **6**, 289–295 (2010).
9. Riegger, L. *et al*. Localized magnetic moments with tunable spin exchange in a gas of ultracold fermions. *Phys. Rev. Lett.* **120**, 143601 (2018).
10. Taie, S., Yamazaki, R., Sugawa, S. & Takahashi, Y. An SU(6) Mott insulator of an atomic Fermi gas realized by large-spin Pomeranchuk cooling. *Nat. Phys.* **8**, 825–830 (2012).

11. Hofrichter, C. *et al*. Direct probing of the Mott crossover in the SU(*N*) Fermi-Hubbard model. *Phys. Rev. X* **6**, 021030 (2016).
12. Scazza, F. et al. Observation of two-orbital spin-exchange interactions with ultracold SU(*N*)-symmetric fermions. *Nat. Phys.* **10**, 779–784 (2014); corrigendum 11, 514 (2015).
13. Cappellini, G. *et al*. Direct observation of coherent interorbital spin-exchange dynamics. *Phys. Rev. Lett.* **113**, 120402 (2014).
14. Höfer, M. *et al*. Observation of an orbital interaction-induced Feshbach resonance in ^{173}Yb. *Phys. Rev. Lett.* **115**, 265302 (2015).
15. Pagano, G. *et al*. Strongly interacting gas of two-electron fermions at an orbital Feshbach resonance. *Phys. Rev. Lett.* **115**, 265301 (2015).
16. Hammer, H.-W., Nogga, A. & Schwenk, A. Colloquium: Three-body forces: from cold atoms to nuclei. *Rev. Mod. Phys.* **85**, 197–217 (2013).
17. Johnson, P. R., Blume, D., Yin, X. Y., Flynn, W. F. & Tiesinga, E. Effective renormalized multi-body interactions of harmonically confined ultracold neutral bosons. *New J. Phys.* **14**, 053037 (2012); corrigendum 20, 079501 (2018).
18. Will, S. *et al*. Time-resolved observation of coherent multi-body interactions in quantum phase revivals. *Nature* **465**, 197–201 (2010).
19. Mark, M. J. *et al*. Precision measurements on a tunable Mott insulator of ultracold atoms. *Phys. Rev. Lett.* **107**, 175301 (2011).
20. Ferlaino, F. *et al*. Efimov resonances in ultracold quantum gases. *Few-Body Syst.* **51**, 113–133 (2011).
21. Fletcher, R. J. *et al*. Two- and three-body contacts in the unitary Bose gas. *Science* **355**, 377–380 (2017).
22. Greene, C. H., Giannakeas, P. & Pérez-Ríos, J. Universal few-body physics and cluster formation. *Rev. Mod. Phys.* **89**, 035006 (2017).
23. D'Incao, J. P. Few-body physics in resonantly interacting ultracold quantum gases. *J. Phys. B* **51**, 043001 (2018).
24. Wolf, J. *et al*. State-to-state chemistry for three body recombination in an ultracold rubidium gas. *Science* **358**, 921–924 (2017).
25. Campbell, S. L. *et al*. A Fermi-degenerate three-dimensional optical lattice clock. *Science* **358**, 90–94 (2017).
26. Marti, G. E. *et al*. Imaging optical frequencies with 100μHz precision and 1.1μm resolution. *Phys. Rev. Lett.* **120**, 103201 (2018).
27. Campbell, G. K. *et al*. Imaging the Mott insulator shells by using atomic clock shifts. *Science* **313**, 649–652 (2006).
28. Kato, S. *et al*. Laser spectroscopic probing of coexisting superfluid and insulating states of an atomic Bose–Hubbard system. *Nat. Commun.* **7**, 11341 (2016).
29. Zang, X.-P., Yang, M., Ozaydin, F., Song, W. & Cao, Z.-L. Generating multiatom entangled *W* states via light-matter interface based fusion mechanism. *Sci. Rep.* **5**, 16245 (2015).
30. Martinez de Escobar, Y. N. *et al*. Two-photon photoassociative spectroscopy of ultracold ^{88}Sr. *Phys. Rev. A* **78**, 062708 (2008).
31. Burt, E. A. *et al*. Coherence, correlations, and collisions: what one learns about Bose-Einstein condensates from their decay. *Phys. Rev. Lett.* **79**, 337–340 (1997).
32. Söding, J. *et al*. Three-body decay of a rubidium Bose-Einstein condensate. *Appl. Phys. B* **69**, 257–261 (1999).
33. Wang, J., D'Incao, J. P., Wang, Y. & Greene, C. H. Universal three-body recombination via resonant d-wave interactions. *Phys. Rev. A* **86**, 062511 (2012).

Acknowledgements We acknowledge technical contributions from W. Milner, E. Oelker, J. Robinson, L. Sonderhouse and W. Zhang, and discussions with T. Bothwell, S. Bromley, C. Kennedy, D. Kedar, S. Kolkowitz, M. D. Lukin, A. Safavi-Naini and C. Sanner. This work was supported by NIST, DARPA, W911NF-16-1-0576 through ARO, AFOSR-MURI, AFOSR, NSF-1734006 and NASA. A.G. is supported by a postdoctoral fellowship from the Japan Society for the Promotion of Science and G.E.M. is supported by a postdoctoral fellowship from the National Research Council. J.P.D. acknowledges support from NSF Grant PHY-1607204.

Author contributions A.G., R.B.H., G.E.M., S.L.C. and J.Y. contributed to the experiments. M.A.P., P.S.J., J.P.D. and A.M.R. contributed to the development of the theoretical model. All authors discussed the results, contributed to the data analysis and worked together on the manuscript.

Competing interests The authors declare no competing interests.

Additional information
Supplementary information is available for this paper at https://doi.org/10.1038/s41586-018-0661-6.
Reprints and permissions information is available at http://www.nature.com/reprints.
Correspondence and requests for materials should be addressed to A.G. and J.Y.
Publisher's note: Springer Nature remains neutral with regard to jurisdictional claims in published maps and institutional affiliations.

METHODS

State preparation. At the end of a 10-s evaporation, a ten-spin-component Fermi gas is loaded into a cubic state-independent optical lattice in a two-stage ramp. The first, 300-ms ramp to about $5E_{rec}$ is used consistently for all the measurements shown. To prepare for $n=4$ and $n=5$ occupied sites, the second ramp to the final lattice depth is sped up from 200 ms to 50 ms to minimize three-body loss during the loading process. n-occupied sites are randomly filled with n different nuclear-spin components from the $\binom{10}{n}$ nuclear-spin configurations. The initial entropy per particle in the lattice is estimated to be $s/k_B=1.8$ (k_B, Boltzmann constant) from the T/T_F measured in the dipole trap before and after lattice loading. In the atomic limit, in which tunnelling is negligible, the maximum spin entropy for $n=1$ sites is $s_{spin}/k_B=\ln(10)=2.3$ for ten spin states. This leads to a lowered temperature in the lattice when entropy is transferred from the motional to the spin degree of freedom[10,11].

To minimize a systematic shift due to the inhomogenity of the trap depth across the cloud, we prepare a $10\,\mu m \times 10\,\mu m \times 2\,\mu m$ sample of sites with the desired occupation by optimizing the final evaporation point. For each image, we measure the spectroscopic response in only the $4\,\mu m \times 4\,\mu m$ region at the centre of the lattice. As the on-site frequency shifts for large occupations increase, the line shapes become asymmetric owing to the residual inhomogeneity of the trap depth. To determine the peak frequencies, we fit each spectrum with an asymmetric Lorentzian, as shown in Fig. 2a. The trap depth in the central region of the lattice is calibrated by motional sideband spectroscopy of an $n=1$ sample, using the same procedure.

Data availability

The data that support the findings of this study are available within the paper.